NANO EXPRESS

Self-assembly of Silver Nanoparticles and Multiwall Carbon Nanotubes on Decomposed GaAs Surfaces

S. H. Al-Harthi · K. P. Revathy · F. Gard ·
A. Mesli · A. K. George · J. Bartringer ·
M. Mamor · N. V. Unnikrishnan

Abstract Atomic Force Microscopy complemented by Photoluminescence and Reflection High Energy Electron Diffraction has been used to study self-assembly of silver nanoparticles and multiwall carbon nanotubes on thermally decomposed GaAs (100) surfaces. It has been shown that the decomposition leads to the formation of arsenic plate-like structures. Multiwall carbon nanotubes spin coated on the decomposed surfaces were mostly found to occupy the depressions between the plates and formed boundaries. While direct casting of silver nanoparticles is found to induce microdroplets. Annealing at 300°C was observed to contract the microdroplets into combined structures consisting of silver spots surrounded by silver rings. Moreover, casting of colloidal suspension consists of multiwall carbon nanotubes and silver nanoparticles is observed to cause the formation of 2D compact islands. Depending on the multiwall carbon nanotubes diameter, GaAs/multiwall carbon nanotubes/silver system exhibited photoluminescence with varying strength. Such assembly provides a possible bottom up facile way of roughness controlled fabrication of plasmonic systems on GaAs surfaces.

Keywords Nanomaterials · Self-assemble · Nanotubes · Ag · GaAs

S. H. Al-Harthi (✉) · K. P. Revathy · F. Gard ·
A. K. George · M. Mamor
Physics Department, College of Science, Sultan Qaboos
University, P.O. Box 36, Al Khod 123, Oman
e-mail: salim1@squ.edu.om

K. P. Revathy · N. V. Unnikrishnan
School of Pure and Applied Physics, Mahatma Gandhi
University, Kottayam 686 560, Kerala, India

A. Mesli
IM2NP, UMR 6242 CNRS, Université Aix-Marseille,
Av. Normandie-Niemen, 13397 Marseille Cedex 20, France

J. Bartringer
Institut d'Electronique du Solide et des Systèmes,
CNRS/ULP, Strasbourg, France

Introduction

Recently, metals have been intensively studied beyond their reflecting nature by exploiting the collective oscillations of their free electrons in the field called plasmonics [1, 2]. The interaction between free electrons and light, inducing resonant modes, refer as plasmons. Well-established techniques have been realized enabling the development of structures to fully exploit these modes [3–7]. Depending on the properties of the supporting structure, plasmons can be broadly divided into two categories: surface and localized surface plasmon resonance (LSPR). Among others, individual colloidal particles with different shape, size and aggregation determine the LSPR modes [8, 9]. For example, by simply adjusting the size and the shape of the metallic nanoparticles, the frequency at which the localized surface plasmon resonance occurs can be tuned from ultraviolet to infrared region of the electromagnetic spectrum [10–12]. GaAs surfaces have been utilized as high index matrices to lower the metallic localized surface resonance frequencies to near-infrared for telecommunication applications [13, 14]. Arsenic (As) precipitates on GaAs surfaces were found to cause strong damping of the surface plasmon modes and, providing absorption of wavelengths longer than 1.5 μm [13]. Fractal aggregates [15, 16] of nanoparticles where local fields are concentrated can lead to interesting optical phenomena and applications such as harmonic generation, Kerr effect [17]

and surface-enhanced Raman scattering (SERS) [9, 18–22]. Experimental studies on plasmon resonance of silver (Ag) nanoparticles on highly ordered pyrolytic graphite (HOPG) [23], diamond-like carbon [24] and fullerene C_{70} matrices [25] all lead to fruitful clues of the possible effects of multiwall carbon nanotubes (MWCNTs) in plasmonic system. In addition to the well-known collective excitations of the π-band electrons in MWCNTs [26, 27], their incorporation in any system can be exploited to design hybrid plasmonic system, either by functionalization of Ag nanoparticles on MWCNTs [28] or by direct filling of MWCNTs with Ag nanoparticles [29].

Motivated by the respective advantages of adjusting size and shape of the Ag nanoparticles, the benefit of using GaAs as high index matrix and coupling with MWCNTs, we report on a novel system which considers three components: A decomposed GaAs surface, MWCNTs and Ag nanoparticles. Although, the self-assembly of metallic Ag nanoparticles on smooth surfaces has been extensively studied and well known, the co-growth or coupling of Ag and MWCNTs on rough GaAs decomposed surfaces is yet to be explored. The topics of particular importance addressed in this work are the morphology of MWCNTs/Ag grown on the decomposed GaAs surfaces, the role of solvent evaporation on the growth mechanism of the MWCNTs/Ag nano-patterns and to some extent photoluminescence properties of the GaAs/MWCNTs/Ag system.

Experimental Details

Samples from commercially available single crystal GaAs (100) wafers were employed as source of substrates. The substrates were cleaned with acetone and ethanol followed by etching using a mixture of sulfuric acid (H_2SO_4), hydrogen peroxide (H_2O_2) and water. After etching, the substrates were immediately loaded into the ultra-vacuum preparation chamber and degassed for 48 h at temperature of 200°C prior to an annealing process at 600°C for 30 min. The temperature was measured using an optical pyrometer with an accuracy of ±25°C. Each GaAs substrate was investigated along (110) direction to allow surface structure observations by reflection high energy electron diffraction (RHEED).

Ag nanoparticles and MWCNTs were used as the starting materials to prepare the spin-coated samples. Ag nano-particles with average size of 30 nm and purity of 99.99% were purchased from Xuzhou Hongwu Nanometer Material Co., ltd China. MWCNTs with outer diameter of 8 nm and purity above 95% were supplied by Chengdu Organic Chemicals Co., ltd China. Colloidal suspension of particles (CSP) were prepared with varying concentration of silver and MWCNTs in toluene. The solutions were ultra-sonicated for 15 min, deposited drop wise on the GaAs substrates and spin coated at 8,000 rpm for 30 s. Some of the spin-coated samples were annealed for 30 min at 300°C in a controlled environment.

Surface morphology of the spin-coated samples on the GaAs substrates was investigated by a Nanoscope V Multimode Atomic Force Microscopy (AFM) provided by Veeco Instrument. To minimize the sample damage, AFM imaging was performed in tapping mode, and observations were made with the AFM instrument placed on vibration isolation VT-102 table in order to minimize the effects of vibration. The measurements were taken at well-stabilized room temperature to avoid thermal drift. During the imaging, both the scan rate and the imaging resolution were set at 0.2 Hz and 512 pixels, respectively. Ultra-high resolution tungsten tips purchased from Micro Masch with tip radius <1 nm and back side coated with aluminum were used for the AFM experiments. All tips had a force constant of 75 N/m and a resonance frequency of 400 kHz.

Photoluminescence (PL) measurements were taken at room temperature. The excitation of the samples was achieved by a YAG laser operating at 532 nm owing to a frequency doubler (the natural emission of the YAG laser occurs at 1,064 nm). Using a frequency trippler and appropriate external filters, we extract the third harmonic (355 nm) which is the main PL exciting component, although a weak trace of the second harmonic (532 nm) remains present in the beam. The diameter of the laser spot was 800 μm, and the incidence angle of the incoming laser beam was 45°. The luminescence, collected by spherical mirror, was analyzed in a 5-nm-resolution spectrometer. The spectrometer integrates the PL signal during 5 s. Within this interval of time, the sample is hit by the pulsed laser with a rate of 20 kHz, and this is done 10^5 times. We collect thus 10^5 PL emissions and so the signal is collected even if it has a very short lifetime.

Results and Discussion

GaAs Surface Decomposition and Its Subsequent Dewetting by Toluene

Figure 1a shows the RHEED pattern with sharp spots indicative of rough surface caused by surface diffusion of As atoms. High-resolution AFM image (Fig. 1b) reveals surface decomposition into oval-like plates surrounded by depressions seen in the dark contrast. The surface is densely covered with irregular structures with RMS roughness of 1.8 nm. X-ray photoemission spectroscopy (XPS) and AFM auxiliary experiments suggest that the decomposed surface is As rich. In addition, the plate density and the
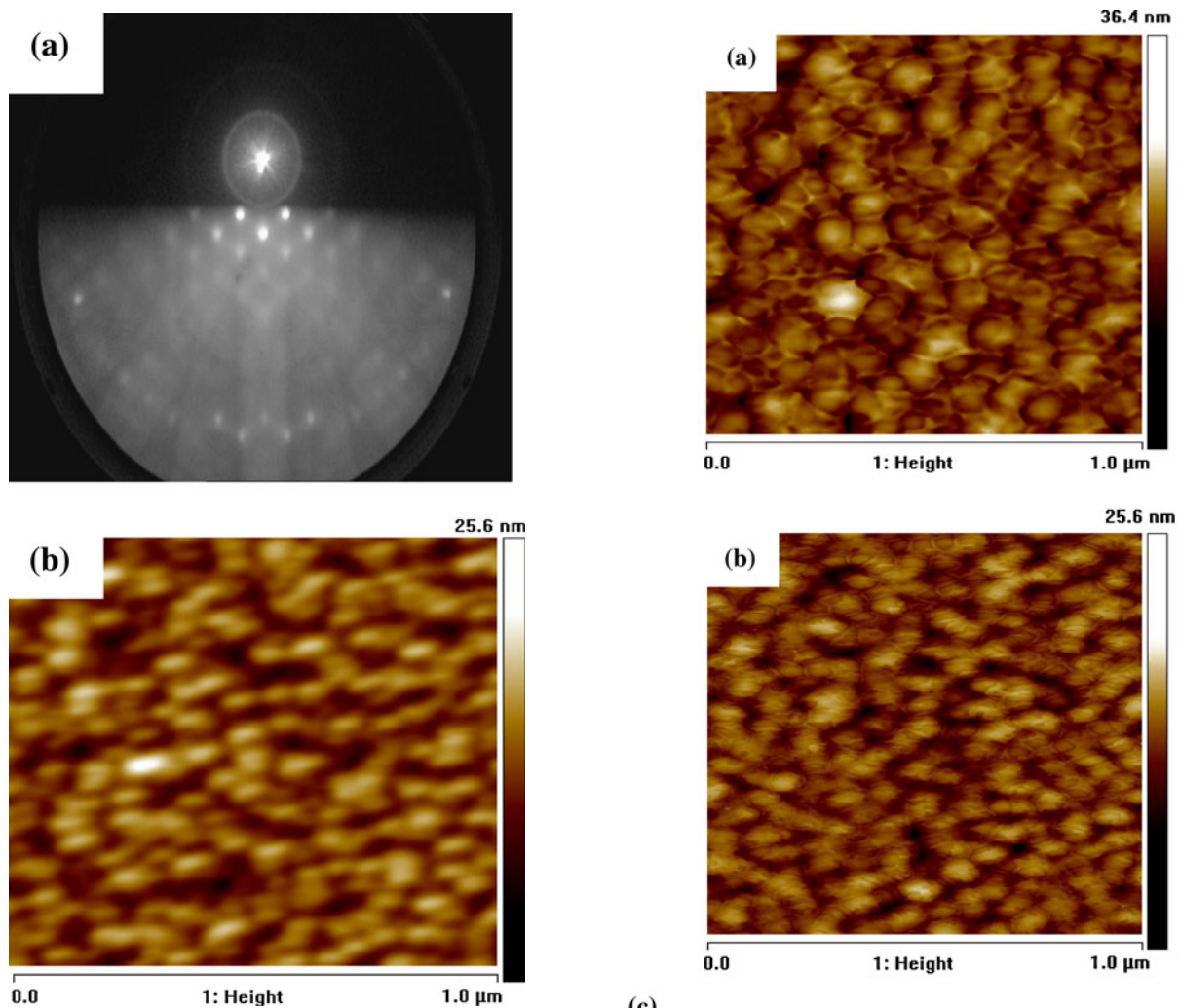
Fig. 1 a RHEED pattern of the decomposed GaAs (100) surface, **b** AFM height image showing oval-like plates formed after thermal surface decomposition

depressions size vary with temperature and annealing time. The decomposed surface proved to be essential where the plates act as templates for the Ag assembly, and the depressions provide free space (sinks) for the MWCNTs to accommodate.

Figure 2a shows a typical wide scan AFM image recorded in the final stages of dewetting of the toluene on the decomposed surface of GaAs. Clearly, toluene forms broken net-like patterns, and sometime hexagonal structures extending over the whole surface occupying the spacing between the plates. Interestingly, the calculated RMS roughness value is 0.2 nm less compared to that found without the toluene (i.e. decomposed surface shown in Fig. 1b). This reduction in the roughness is attributed to the smoothing effect induced by toluene as it fills the depressions.
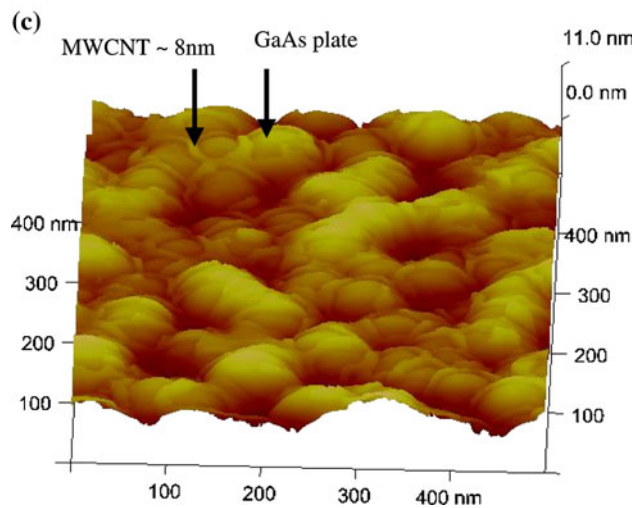

Fig. 2 a A $1 \times 1 \ \mu m^2$ AFM image showing the dewetting of the GaAs substrate by toluene. The dewetting layer is very thin as a result of high speed spin coating of toluene (8,000 rpm); **b** A $1 \times 1 \ \mu m^2$ AFM image showing the assembly of MWCNT on the GaAs substrate. The distribution of the MWCNT resembles to that for the toluene shown in (**a**); **c** represents a 3D AFM image showing the assembly of MWCNT on the GaAs substrate

Assembling of MWCNTs and Ag Nanoparticles on the GaAs Decomposed Surface

Assembling of MWCNTs on the GaAs decomposed surface is shown in Fig. 2b. A MWCNTs net-like pattern similar to that of toluene can be clearly seen. The image shown was attained after desorption of toluene at 300°C for 30 min. Hence, the observed features are only attributed to the MWCNTs with average thickness of 8 nm and the decomposed surface. This is well reflected from the high-resolution 3D image shown in Fig. 2c.

At this point, we turn our discussion to the wetting of the decomposed surface by a colloidal system consisting of 0.1% concentration of Ag nanoparticles dissolved in toluene. The effect of Ag nanoparticles on the toluene wetting behavior and its hydrodynamic is huge. Figure 3a depicts this effect where the wetting by the Ag colloidal particles induces separated array of droplets. Similar droplets have been observed following the wetting of a toluene solution composed of polystyrene and Ag nanoparticles on silicon substrates [30]. The droplets have an average diameter of 1 μm, average distance of 1.9 μm and droplet density of 2.5×10^7 cm^{-2}. To investigate the self-assembly of the Ag nanoparticles within the microdroplet structures, the samples were annealed at 300°C. From Fig. 3b, we notice two types of aggregates formed after annealing: the normal plates of the decomposed GaAs surface and spot structures surrounded by rings (e.g. enclosed by square). Separate spots and empty rings have been reported by Nobuhiko et al. [30] while observing polystyrene and Ag nanoparticles system. To the best of our knowledge, this is the first report on a combination of Ag spot and Ag ring in one structure. Different mechanisms have been proposed for the ring and spot formation (sometimes refereed as aggregates or islands). These are as follows: capillary flow-induced localization along the contact line (the border between the liquid film and the substrate or the three-phase line of the dewetting solution film) [30, 31], capillary flow [32], kinetically driven islands formation [33] and pinning of dewetting hole [34]. Here, we argue that the first three mechanisms are responsible at different stages for the combined structure formation as schematically illustrated in Fig. 4. Initially, we adapt the capillary flow-induced localization along the contact line only to explain the formation of droplets (Fig. 3a) before the evaporation. Firstly, the contact line moves toward the liquid phase and then the Ag nanoparticles are captured by capillary flow and collected at contact line forming a sinusoidal interface leading to the microdroplets formation (Fig. 4a, b, c). Once the evaporation starts, the droplets shrink due to the annealing of the sample. This is reinforced by the fact that the observed size of the droplet is four times larger compared to that of the combined structure as shown in Fig. 3c. At this stage, two
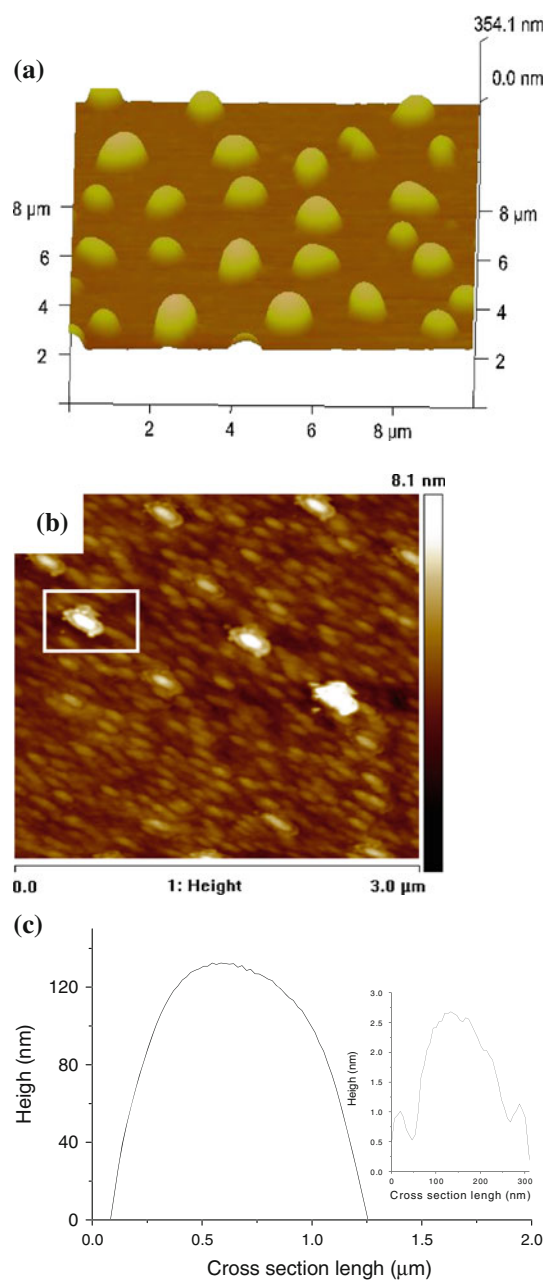
Fig. 3 **a** 3D AFM image of the droplet formation upon casting of a colloidal system consisting of 0.1% concentration Ag nanoparticles dissolved in toluene and spin coated at 8,000 rpm; **b** AFM image shows two types of structures: plates and Ag spots surrounded by rings (e.g. enclosed by *square*) induced after the evaporation of toluene at 300°C for 30 min; **c** A cross-section profile showing ≈ 1.2 μm diameter droplet size. The *inset* shows a cross-section profile of the combined structure with ≈ 310 nm diameter size

simultaneous events are taking place as shown in Fig. 4d, e. These events are very fast to be experimentally detected by many techniques including AFM used in this work. Therefore, here we provide only theoretically grounded [32, 33] explanation without any direct evidence of their occurrence. The first event is the compensation by outward flow to
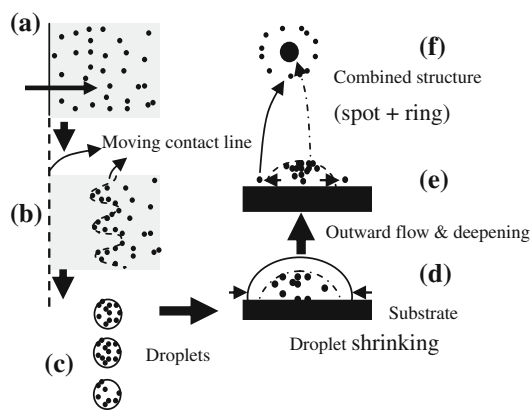
Fig. 4 A proposed mechanism of the combined structure formation. **a** Ag particles in toluene; **b** movement of contact line and the development of a sinusoidal interface where particles are captured; **c** droplet formation; **d** droplets shrinking (not to scale); **e** Outward flow and deepening of particles toward the substrate; **f** spot formation due to the deposition of the particles on the substrate and ring formation due the outward compensation

restore the shrinkage (capillary flow mechanism) and deepening of the solvent–air interface of the contracted droplet. As the evaporation continues, the contact line recedes and lays its accumulated particles (kinetically driven islands formation mechanism as shown in Fig. 4d) on the substrate to form the spot structure, and the outward flow forms the ring surrounding the spot as indicated in Fig. 4f.

Next, we attempt to examine a complete system consisting of Ag and MWCNTs on the decomposed GaAs surface. Figure 5a shows the AFM image of such system after annealing of the sample at 300°C for 30 min. Spherical droplets and combined structures such as those found and shown in Fig. 3a, b are not any more observed. Instead, the film breaks into remarkable compact 2D Ag islands seen on the top of arsenic plate and surrounded by MWCNTs.

Decomposition Effects on the Assembly of MWCNTs and Ag Nanoparticles

In order to quantify our observations and to investigate the effects of surface decomposition on the assembly of MWCNTs and Ag nanoparticles, PSD analysis was carried out. Figure 5b represents the PSD profiles of these systems. Both low and high spatial frequency regions of the PSD have been influenced by the different sample preparation conditions. However, in the high frequency region all systems obey the inverse power law (fractal model) indicating a strong presence of fractal components (i.e. the effect of As plates in all systems) and given by [35],

$$PSD_{fractal} = \frac{K}{f^{v+1}} \tag{1}$$

where f is the frequency, v and K are the spectral indices and spectral strength, respectively. In addition, the slope of

the PSD at this region is almost the same indicating the same fractal spectral indices (v) value of 5.1. Since v is related to the roughness exponent (α) by the equation $\alpha = (v - d)/2$ [36], where the line scan dimension d is 2, $\alpha = (5.1–2)/2 = 1.5$. The high frequency PSD analysis supports the idea that the plates have strong influence on the distribution of MWCNTs and toluene. As seen from the PSD, the low frequency parts vary and represent predominantly the aggregates. Both decomposed GaAs/ Toluene and decomposed GaAs/MWCNTs system show 'knee' features (indicated by arrows) in PSD profiles at the interface between the two frequency regions. Their presence indicates aggregation of either toluene or MWCNTs at the depressions as observed in the AFM images shown in Fig. 2a, b. These features are absent in the decomposed GaAs surface. Apart from substrate's fractals (plates), the aggregates in the depressions can be considered as fractals developed during the growth stage. In this case, these extra fractals can be described by the ABC model which is given by [37],

$$PSD_{ABC} = \frac{A}{(1 + B^2 f^2)^{(C+1)/2}} \tag{2}$$

with A, B, C being parameters involved in describing the RMS roughness and the correlation length in wide frequency range. The PSD profile for the GaAs/Toluene system shown in the inset of Fig. 5b is indeed well fitted with this model.

A Proposed Model for the Growth of GaAs/MWCNTs/ Ag System

Based on AFM experimental observations and PSD data analysis, a conceptual growth model of GaAs/MWCNTs/ Ag system is proposed and schematically illustrated in Fig. 6. Once the substrate is etched, its surface decomposes into plates due to the thermal treatment. The density and the spacing between the plates depend on the decomposition temperature and time. Upon spin coating, the majority of MWCNTs dissolved in toluene occupying the spacing and act as boundaries to isolate the plates. If Ag nanoparticles are deposited directly on decomposed substrate without MWCNTs, combined structures (spots + rings) are formed. However, incorporation of MWCNTs cause the Ag to form compact assembly of Ag islands as observed in Fig. 5a and illustrated in Fig. 6d.

Photoluminescent Properties

Figure 7 shows the PL spectra measured at room temperature for the different components in the GaAs/MWCNTs/ Ag system. The intensity of the PL spectra shows both photoluminescence enhancement and quenching of the
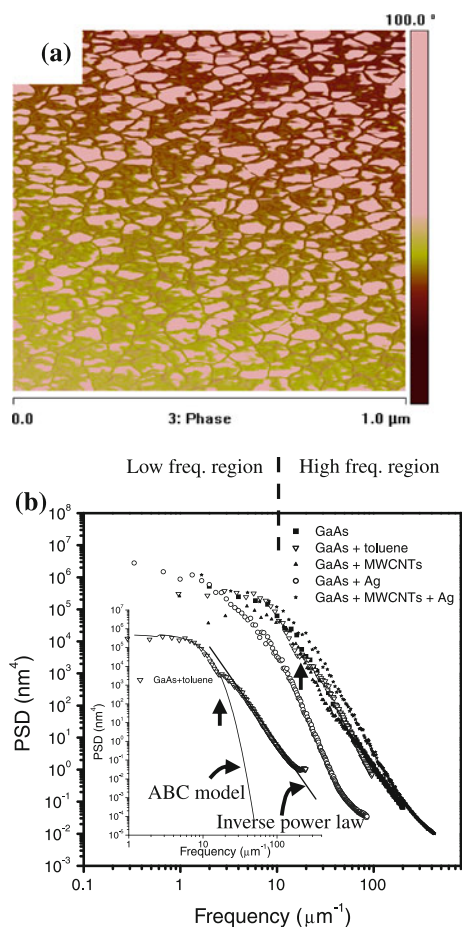
Fig. 5 a AFM phase image showing the decomposed GaAs substrate by a colloidal solution which consists of MWCNTs and Ag nanoparticles after annealing at 300°C for 30 min. Compact 2D island self-assembly of Ag and possible GaAs are seen in the image, **b** experimental PSD profiles of the decomposed GaAs, decomposed GaAs/Toluene and decomposed GaAs/MWCNTs annealed at 300°C. The *inset* is the PSD of the GaAs/Toluene system fitted by the fractal and ABC models

Fig. 7 Photoluminescence spectra from different components of the GaAs/MWCNTs/Ag system excited at 532 nm at room temperature. The *inset* shows the PL peaks from GaAs

lead to an enhancement of optical response [29]. The PL of GaAs/MWCNTs/Ag system can be tuned by varying the diameter of MWCNTs, though the dependency mechanism of the tube diameter with optical response is still unclear. From Fig. 7, the silver nanoparticles PL signal was found to be around 400 nm, and the addition of MWCNTs to the silver/GaAs system resulted in the intensity variation. It is also observed that the emission peak energy of the silver nanoparticles shifts from 3.12 eV (397 nm) to 3.2 eV (387 nm), i.e. inclusion of MWCNTs of higher diameter ($\approx$50 nm) into GaAs/Ag system results in a blue shift in the emission peak energy with reduction in the intensity of the PL spectrum. It is worth mentioning at this stage that although light emission, resulting for surface plasmons, may have very short life time, its effect on the PL signal can be caught by the spectrometer when operating in appropriate conditions as detailed in the Sect. "Experimental Details". The peaks indicated by arrows in Fig. 7 could possibly be attributed to the coupling between MWCNTs and Ag nanoparticles, similar to that reported for Au/MWCNTs system [38]. Regardless of the silver MWCNTs coupling, PL peaks of high index decomposed GaAs matrix presented in the inset of Fig. 7 show a slight

GaAs/MWCNTs/Ag system. The PL enhancement is obtained with the incorporation of MWCNTs of diameter 8 nm, whereas quenching is observed with the use of MWCNTs of diameter ~50 nm. Our results match with theoretical studies predicting that carbon nanotubes, used as spectroscopic enhancers, filled with Ag nanoparticles

Fig. 6 Schematic representation of the proposed growth model of GaAs/MWCNT/Ag system: **a** etched GaAs (100) substrate; **b** Surface decomposition of the sample annealed at 600°C; **c** MWCNTs occupying depressions between As plates; **d** final structure after deposition of Ag nanoparticles and annealing at 300°C
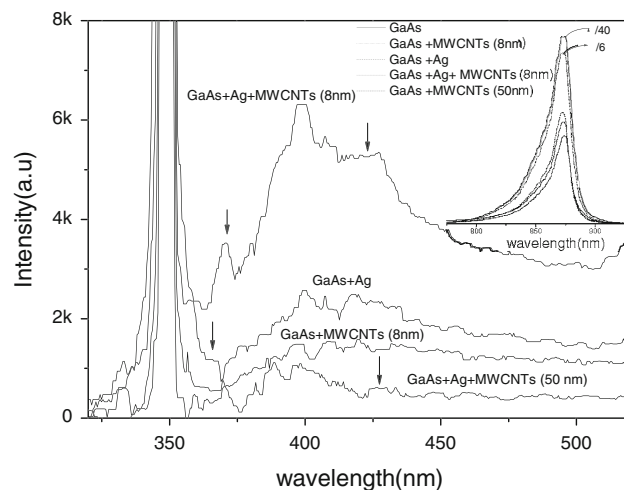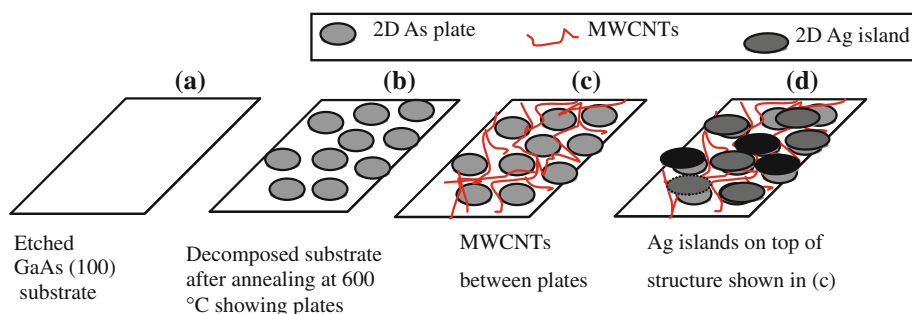
red-shift with reduction in the PL intensity of the well-known GaAs peak around 870 nm [29]. This reduction is due to the fact that GaAs matrix is partially covered by either silver nanoparticles or MWCNTs. Hence, large electron diffusion length of surface deposited Ag on the GaAs surface causes a decrease in the number of electrons useful for recombination processes. The reason for red-shift needs more exploration to check whether quantum confinement effect of decreasing particle size is the only determining factor [39].

Summary

This contribution shade light on the GaAs/MWCNTs/Ag sample preparation and its self-assembled structures. PSD data analysis suggested strong fractal effects of the decomposed surfaces on the successive MWCNTs and toluene layers. Depending on the MWCNTs diameter, the GaAs/MWCNTs/Ag system exhibits enhanced photoluminescence when MWCNTs diameter is 8 nm, while quenching and blue shift are dominant for the higher diameter (≈ 50 nm) MWCNTs. However, possible contribution of As-platelets or Ag-oxide to the PL needs further investigation. In addition, comprehensive and quantitative picture is yet to emerge to understand the physics of interaction between different components in the system. In particular, issues such as the impact of the decomposed surface and the MWCNTs diameter PL signal dependent mechanism deserved more attention.

References

1. W.A. Murray, W.L. Barnes, Adv. Mater. **19**, 3771 (2007)
2. I. Lundstrom, Biosens. Bioelectron. **9**, 725 (1994)
3. T.R. Jensen, M.D. Malinsky, C.L. Haynes, R.P. Van Duyne, J. Phys. Chem. B **104**, 10549 (2000)
4. A. Sundaramurthy, P.J. Schuck, N.R. Conley, D.P. Fromm, G.S. Kino, W.E. Moerner, Nano Lett. **6**, 355 (2006)
5. S.I. Bozhevolnyi, V.S. Volkov, E. Devaux, J.-Y. Laluet, T.W. Ebbesen, Nature **440**, 508 (2006)
6. T.W. Ebbesen, H.J. Lezec, H.F. Ghaemi, T. Thio, P.A. Wolff, Nature **391**, 667 (1998)
7. H. Ditlbacher, J.R. Krenn, G. Schider, A. Leitner, F.R. Aussenegg, Appl. Phys. Lett. **81**, 1762 (2002)
8. C.L. Nehl, H. Liao, J.H. Hafner, Nano Lett. **6**, 683 (2006)
9. V.M. Shalaev, R. Botet, R. Jullien, Phys. Rev. B **44**(12), 216 (1991)
10. K.L. Kelly, E. Coronado, L.L. Zhao, G.C. Schatz, J. Phys. Chem. B **107**, 668 (2003)
11. Z. Liu, H. Wang, H. Li, Appl. Phys. Lett. **72**, 1823 (1998)
12. H. Mertens, J. Verhoeven, A. Polman, Appl. Phys. Lett. **85**, 1317 (2004)
13. D.D. Nolte, J. Appl. Phys. **76**, 3740 (1994)
14. S. Okamoto, Y. Kanemitsu, K. Sung Min, H.A. Atwater, Appl. Phys. Lett. **73**, 1829 (1998)
15. K.H. Su, Q.H. Wei, X. Zhang, J.J. Mock, D.R. Smith, S. Schultz, Nano Lett. **3**, 1087 (2003)
16. M. Quinten, J. Cluster Sci. **10**, 319 (1999)
17. V.M. Shalaev, *Nonlinear Optics of Random Media: Fractal Composites and Metal-Dielectric Films, Vol 158 of Springer Tracts in Modern Physics* (Springer, 2000)
18. M. Moskovits, Rev. Mod. Phys. **57**, 783 (1985)
19. H.H. Wang, C.Y. Liu, S.B. Wu, N.W. Liu, C.Y. Peng, T.H. Chan, C.F. Hsu, J.K. Wang, Y.L. Wang, Adv. Mater. **18**, 491 (2006)
20. K. Kneipp, Y. Wang, H. Kneipp, L.T. Perelman, I. Itzkan, R. Dasari, M.S. Feld, Phys. Rev. Lett. **78**, 1667 (1997)
21. S.M. Nie, S.R. Emery, Science **275**, 1102 (1997)
22. C.L. Haynes, R.P. Van Duyne, J. Phys. Chem. B **107**, 7426 (2003)
23. M. Merschdorf, W. Pfeiffer, A. Thon, S. Voll, G. Gerber, Appl. Phys. A **71**, 547 (2000)
24. S. Hussain, R.K. Roy, A.K. Pal, Mat. Chem. Phys. **99**, 375 (2006)
25. R. Singhal, D.C. Agarwal, Y.K. Mishra, F. Singh, J.C. Pivin, R. Chandra, D.K. Avashi, J. Phys. D Appl. Phys. **42**, 155103 (2009)
26. L.A. Bursill, P.A. Stadelmann, J.L. Peng, S. Prawer, Phys. Rev. B **49**, 2882 (1994)
27. M.F. Lin, K.W. Shung, Phys. Rev. B **50**, 17744 (1994)
28. M.A. Correa-Duarte, M. Liz-Marzán, J. Mater. Chem. **16**, 22 (2006)
29. F.J. Garcia-Vidal, J.M. Pitarke, J.B. Pendry, Phys. Rev. B **58**, 6783 (1998)
30. N.J. Suematsu, Y. Ogawa, Y. Yamamoto, T. Yamaguchi, J. Colloid Interface Sci. **310**, 648 (2007)
31. K. Kaga, K. Okamoto, T. Echizen, O. Karthaus, K. Nakajima, Kbunshi Ronbunshu **60**, 752 (2003)
32. R.D. Deegan, O. Bakajin, T.F. Fupont, G. Huber, S.R. Nagel, T.A. Witten, Nature **389**, 827 (1997)
33. T.P. Bigion, X.M. Lin, T.T. Nguyen, E.I. Corwin, T.A. Witten, H.M. Jaeger, Nat. Mater. **5**, 265 (2006)
34. P.C. Ohara, W.M. Gelbart, Langmuir **14**, 3418 (1998)
35. E.L. Church, Appl. Opt. **22**, 1518 (1988)
36. M.M. Hawkeye, M.J. Brett, J. Vac. Sci. Technol. A **25**, 1317 (2007)
37. G. Palasantzas, Phys. Rev. B **48**, 14472 (1993)
38. R. Zhou, M. Shi, X. Chen, M. Wang, Y. Yang, X. Zhang, H. Chen, Nanotechnology **18**, 485603 (2007)
39. A. Longo, G.P. Pepe, G. Carotenuto, A. Ruotolo, S. De Nicola, V.I. Belotelov, A.K. Zvezdin, Nanotechnology **18**, 36570 (2007)